6

VALIDATION AND VERIFICATION

6.1 INTRODUCTION

This chapter presents a comparison of the newly developed Multi-sphere Unit Cell Model results with various experimental results. The Multi-sphere Unit Cell and various other models where implemented in Engineering Equation Solver (EES) to obtain simulation results and can be found in Appendix G. The experimental data was chosen in order to validate all the separate effects contributing to heat transfer in a randomly packed bed. The separate effects, conduction and radiation in the bulk and wall regions, are generally verified using: (1) the spherical-flat contact experimental facility (Section C.1); (2) the spherical-spherical experimental facility (Section C.2); and (3) the High Temperature Oven (HTO) experimental test facility (Section C.3). In addition, the SANA-I experimental test facility constructed and operated at the Research Centre in Jülich in Germany (Section C.4) and the HTTU experimental test facility constructed and operated at the North-West University in Potchefstroom was used to verify the integrated heat transfer effects in all the regions defined in a randomly packed bed. Summaries of the experimental tests used are presented in Table 6.1 to Table 6.3.

Table 6.1: Experimental tests used for the validation of the Multi-sphere Unit Cell Model in the bulk region

THERMAL PHENOMENON	RESEARCHER/S	PACKING TYPE	ENVIRONMENT	TEST SPECIMEN & PARAMETERS	SPHERE SIZE	MEAN BULK POROSITY
SEPARATE EFFECTS IN BULK REGION						
CONDUCTION (BULK)	Buonanno *et al.* (2003:251)	SC FCC	Air 1atm Pressure, 101.358 kPa	100Cr6 Steel spheres	$d_p = 19.05mm$ $d_p = 19.05mm$	$\varepsilon = 0.476$ $\varepsilon = 0.2595$
RADIATION (BULK)	Robold (1982:156) Breitbach & Barthels (1980:392)	Random, Bulk Region	Vacuum	Graphite	$d_p = 40mm$	$\bar{\varepsilon} = 0.39$
INTEGRATED EFFECTS IN BULK REGION						
CONDUCTION + RADIATION (BULK)	Robold (1982:156)	Random, Bulk Region	Helium 70 kPa - 85 kPa	Graphite	$d_p = 40mm$	$\bar{\varepsilon} = 0.39$

Table 6.2: Experimental tests used for the validation of the Multi-sphere Unit Cell Model in the wall region

THERMAL PHENOMENON	RESEARCHER/S	ENVIRONMENT	TEST SPECIMEN & PARAMETERS	SPHERE SIZE
SEPARATE EFFECTS IN WALL REGION				
CONDUCTION (WALL)	Kitscha & Yovanovich (1974:93)	$0.5d_p$ from wall Argon, 0.073 kPa – 98.67 kPa	Carbon steel sphere, Flat 1020 steel	$d_p = 25.4mm$
RADIATION (WALL)	Robold (1982:156) Breitbach & Barthels (1980:392)	$0.5d_p$ from wall Vacuum	Graphite sphere Flat graphite	$d_p = 40mm$
INTEGRATED EFFECTS IN WALL REGION				
CONDUCTION + RADIATION (WALL)	Robold (1982:156) Breitbach & Barthels (1980:392)	$0.5d_p$ from wall Helium 70 kPa - 85 kPa	Graphite sphere Flat graphite	$d_p = 40mm$

Table 6.3: Experimental tests used for the verification of the Multi-sphere Unit Cell Model in the wall, near-wall and bulk regions

THERMAL PHENOMENON	TEST FACILITY	ENVIRONMENT	TEST SPECIMEN & PARAMETERS	SPHERE SIZE
CONDUCTION + RADIATION (WALL, NEAR-WALL AND BULK)	SANA-I	Helium, 1atm = 101.328 kPa	Graphite sphere	$d_p = 60mm$
CONDUCTION + RADIATION (WALL, NEAR-WALL AND BULK)	HTTU	Nitrogen 10 kPa	Graphite sphere	$d_p = 60mm$

6.2 *VALIDATION OF MULTI-SPHERE UNIT CELL IN THE BULK REGION*

In this section, the conduction and radiation components of the Multi-sphere Unit Cell Model in the bulk region are validated separately and integrally using data obtained by Buonanno *et al.* (2003:251), Robold (1982:154) and Breitbach & Barthels (1980:392).

Buonanno *et al.* (2003:251) conducted experiments to determine the effective thermal conductivity through 100Cr6 steel spheres. Tests were conducted using SC- and FCC-packed structures with air as the interstitial gas at atmospheric conditions. The effective thermal conductivity results were then obtained by varying the root mean square surface roughness σ_{RMS} of the spheres from $0.03\mu m$ to $1.7\mu m$, as well as the average applied force. The experimental setup is shown in Figure C.2.

The first experimental data set of Buonanno *et al.* (2003:251) that is considered is that of the SC packing at a constant applied force of $F = 0.983N$ and the root mean square surface roughness σ_{RMS} varied, as displayed in Table C.4. The effective thermal conductivity between two spheres can be obtained by rewriting Eq. (5.34), in order to account for the SC

packing, with $\bar{\phi}_c = 90^\circ$ and $\bar{n} = 1$, so that $k_e^{g,c}$ is given by:

$$k_e^{g,c} = \frac{\bar{N}_c\left(d_p - \omega_0\right)}{2d_p^2 R_j}\sin\bar{\phi}_c = \frac{\left(d_p - \omega_0\right)}{d_p^2 R_j} \tag{6.1}$$

where R_j can be obtained from Eq. (5.3). The effective thermal conductivity measurements obtained by Buonanno *et al.* (2003:251) were determined by considering the total length of the experiment, that is $L_{bed} = 0.15[m]$. Therefore, the total resistance of the experiment must be calculated. Owing to the structure of the packing, the thermal resistance of the bulk region can be obtained by the following:

$$R_{bulk} = \frac{L}{A_c k_e} = \frac{L_{bulk}}{d_p^2 k_e^{g,c}} \tag{6.2}$$

where the length of the packed bed in the bulk region is $L_{bulk} = \left(0.15 - d_p\right)[m]$. In the experimental setup, there are two wall regions. The thermal resistance between a hemisphere and a wall $R_{j,W}$ is shown in Eq. (5.51), and therefore the effective thermal conductivity for this experimental setup is:

$$k_{e,total}^{g,c} = \frac{L_{bed}}{d_p^2\left(R_{bulk} + 2R_{j,W}\right)} \tag{6.3}$$

where $L_{bed} = 0.15m$. Figure 6.1 displays the comparison between Eq. (6.3) and the data set developed by Buonanno *et al.* (2003:251).

It should be noted that Bahrami *et al.* (2006:3694) suggest that an equivalent radius r_{eq} Eq. (3.116) be used between two spherical surfaces. However, Bahrami *et al.* (2006:3696) also propose that $r_{eq} = r_p$ between two spheres when they compared their model with Buonanno *et al.*'s (2003:251) experimental data set. This, however, is in contrast to his theory, but he stated that it yielded better results.

Nonetheless, the Multi-sphere Unit Cell displays good agreement in Figure 6.1 with the experimental data at low surface roughness. However, it seems that it compares better when $r_{eq} = r_p$ at lower and higher surface roughness. The average percentage difference between the Multi-sphere Unit Cell Model and experimental data with $r_{eq} = r_p$ is 2.96%.

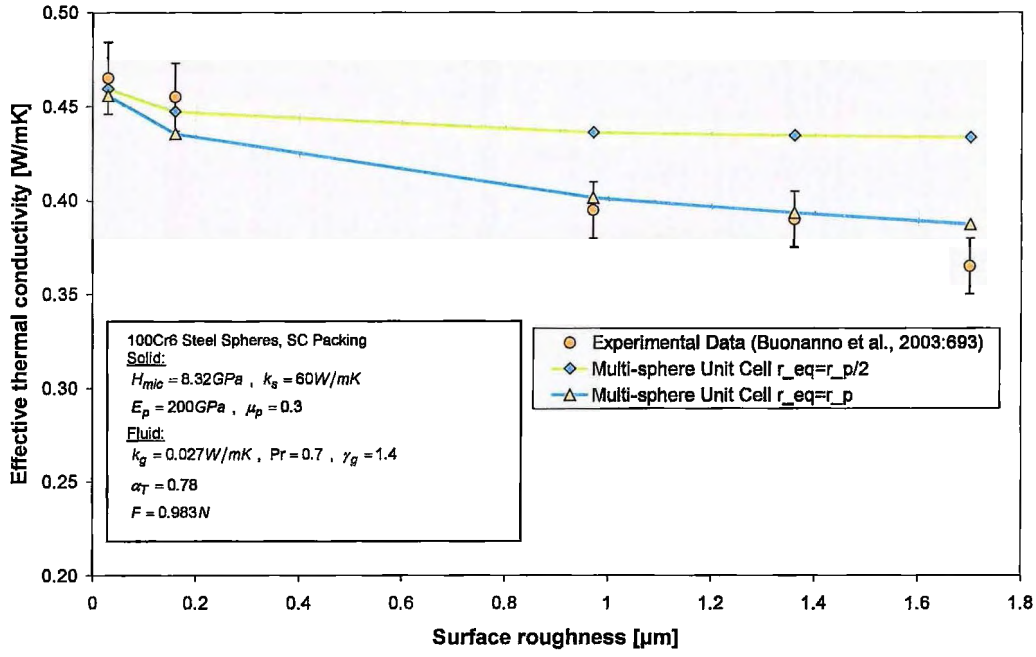

Figure 6.1: Comparison between Multi-sphere Unit Cell Model and Simple Cubic experimental data (Buonanno *et al.*, 2003:251; constant force)

The second experimental data set developed by Buonanno *et al.* (2003:251) that is considered is that where the applied force was varied with a constant root mean square surface roughness in the SC-packing arrangement. Comparison between Eq. (6.3) and experimental data is displayed in Figure 6.2.

It can be seen in Figure 6.2 that the Multi-sphere Unit Cell Model shows good comparison with the experimental data developed by Buonanno *et al.* (2003:251), achieving an average percentage difference of 2.42% when $\sigma_{RMS} = 0.03\,\mu m$ and 5.62% when $\sigma_{RMS} = 1.7\,\mu m$. It is shown that in both cases the Multi-sphere Unit Cell Model falls within the uncertainty bounds. The solid and gas properties used in the simulation results displayed in Figure 6.2 is exactly the same as those displayed in Figure 6.1.

Superimposed on to Figure 6.2, is the effective thermal conductivity obtained when using the Hertzian contact network defined in Eq. (5.4). The Hertzian contact network demonstrates the same trend as its counterparts. However, prediction overestimates the effective thermal conductivity to some extent. This is ascribed to the simplification of the surface roughness to a perfectly smooth contact surface. The rough contact network shows better agreement.

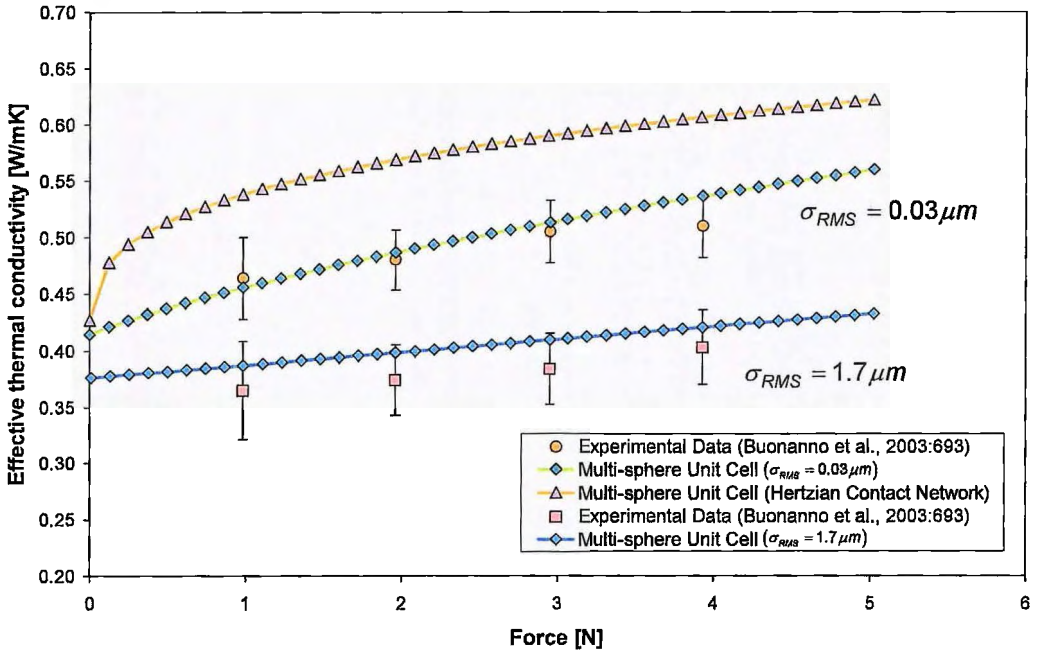

Figure 6.2: Comparison between Multi-sphere Unit Cell Model and Simple Cubic experimental data
(Buonanno *et al.*, 2003:251; constant surface roughness)

The third experimental data set of Buonanno *et al.* (2003:251) that is considered is that of the FCC packing with a constant applied force of $F = 0.783N$ and varying the root mean square surface roughness σ_{RMS}, as displayed in Table C.4. The effective thermal conductivity between two spheres in the FCC setup can be obtained by rewriting Eq. (5.34), in order to account for the FCC packing, with $\bar{\phi}_c = 45°$ and $\bar{n} = 4$, as was displayed in Table 3.2, so that $k_e^{g,c}$ is given by:

$$k_e^{g,c} = \frac{4\left(d_p - \omega_0\right)}{d_p^2 R_j} \sin\left(45°\right) \tag{6.4}$$

where R_j is given by Eq. (5.3). As previously mentioned, the effective thermal conductivity measurements obtained by Buonanno *et al.* (2003:251) was determined by considering the total length of the experiment and, therefore, the total resistance of the experiment must be calculated. However, in contrast to the SC packing, a different conduction area in a FCC-packing structure must be considered, which is displayed in Figure 6.3.

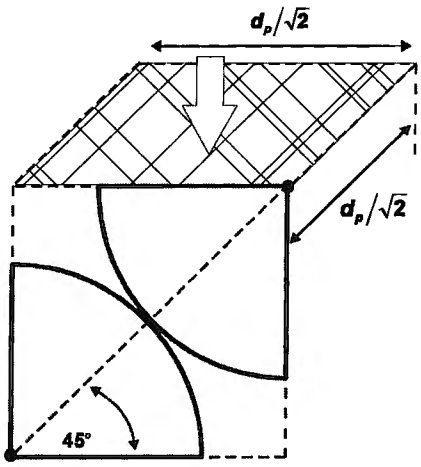

Figure 6.3: Face-centred Cubic conduction area

The thermal resistance of the bulk region can then be calculated by the following:

$$R_{bulk} = \frac{L}{A_c k_e} = \frac{2L_{bulk}}{d_p^2 k_e^{g,c}} \tag{6.5}$$

where the length of the packed bed in the bulk region is $L_{bulk} = \left(0.15 - d_p\right)[m]$. Again, the wall region must be taken into account with $R_{j,W}$ as given by Eq. (5.51). The effective thermal conductivity for this experimental can therefore be calculated by:

$$k_{e,total}^{g,c} = \frac{L_{bed}}{d_p^2\left(R_{bulk} + 2R_{j,W}\right)} \tag{6.6}$$

where $L_{bed} = 0.15m$. Figure 6.4 displays the comparison between Eq. (6.6) and the data developed for the FCC packing by Buonanno *et al.* (2003:251).

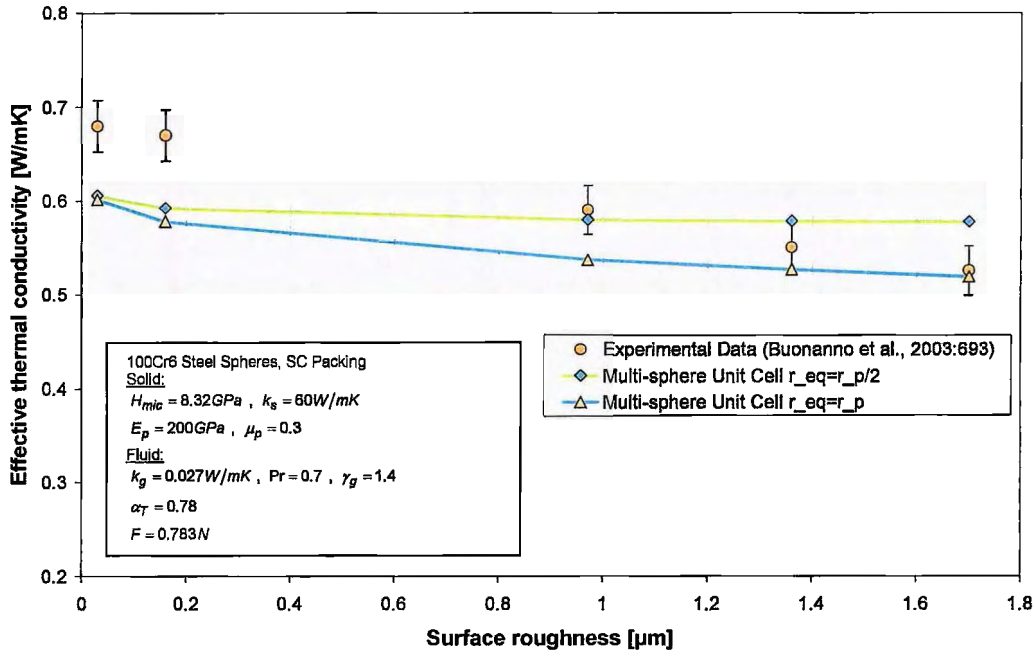

Figure 6.4: Comparison between Multi-sphere Unit Cell Model and Face-centred Cubic experimental data
(Buonanno *et al.*, 2003:251; constant force)

The same comparison regarding the equivalent radius as done in Figure 6.1 is demonstrated for the FCC packing in Figure 6.4. Although both cases deviate from experimental data at the lower surface roughness regions, better comparison is obtained at higher surface roughness. It is therefore concluded in this study that $r_{eq} = r_p$ for both the wall and bulk regions. The average percentage difference between the Multi-sphere Unit Cell Model and experimental data with $r_{eq} = r_p$ is 8.9%.

The fourth experimental data set developed by Buonanno *et al.* (2003:251) that is considered is that of varying the applied force with a constant root mean square surface roughness in a FCC-packing arrangement. The comparison between Eq. (6.6) and experimental data is displayed in Figure 6.5.

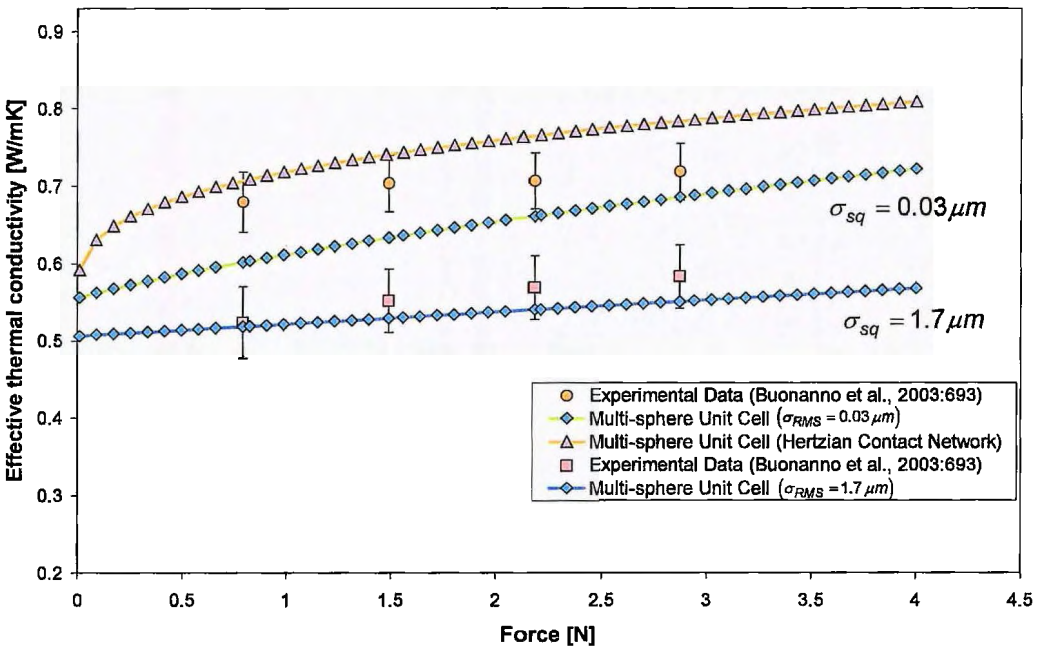

Figure 6.5: Comparison between Multi-sphere Unit Cell Model and Face-centred Cubic experimental data (Buonanno *et al.*, 2003:251; constant surface roughness)

It can be seen in Figure 6.5 that the Multi-sphere Unit Cell Model shows relatively good comparison with the experimental data developed by Buonanno *et al.* (2003:251), achieving an average percentage difference of 8.85% when $\sigma_{RMS} = 0.03\,\mu m$ and 4.08% for when $\sigma_{RMS} = 1.7\,\mu m$. The solid and gas properties used in the simulation results displayed in Figure 6.5 are exactly the same as that displayed in Figure 6.4.

It must be mentioned at this point that typical surface roughness of a graphite pebble after manufacturing or after passing through the reactor is not available and such data should be required for further simulations.

The next experimental data set that is considered is that developed using the HTO experimental test facility (Breitbach & Barthels, 1980:392; Robold, 1982:156). The HTO experimental test facility consisted of a cylindrical graphite vessel containing the randomly packed bed of spheres with diameter $d_p = 0.04\,m$. The cylindrical vessel had a diameter of $0.5m$ and a height of $0.7m$ (Section C.3). An induction-heating coil, situated outside the cylindrical packed bed added heat to the bed. The effective thermal conductivity was extracted using a transient method as explained in Breitbach & Barthels (1980:392). However, the use of a single porosity to characterise the whole packing can be questioned. Nonetheless, tests were conducted at vacuum and elevated pressures.

The first experimental setup that is considered is the test conducted at vacuum conditions with graphite spheres up to a temperature of almost 1600°C. Due to the small size of the cylindrical packed bed, it is assumed as Breitbach & Barthels (1980:395) did, that the heat transfer only occurred through thermal radiation and that point contact conduction is negligible.

To validate this assumption, a parametrical study with the Multi-sphere Unit Cell Model is done at an elevated helium gas pressure $(1atm - 85\,kPa)$. Results shown in Figure 6.6 verifies that heat transfer mostly occurs through the bulk gaseous region rather than the point contact region as contact thermal resistance is much higher that gas thermal resistance. This indicates that at vacuum conditions heat will be transferred more easily by other methods such as thermal radiation rather than being transferred through point contact conduction. The material properties used in this parametrical study are the same as presented in Figure 6.8.

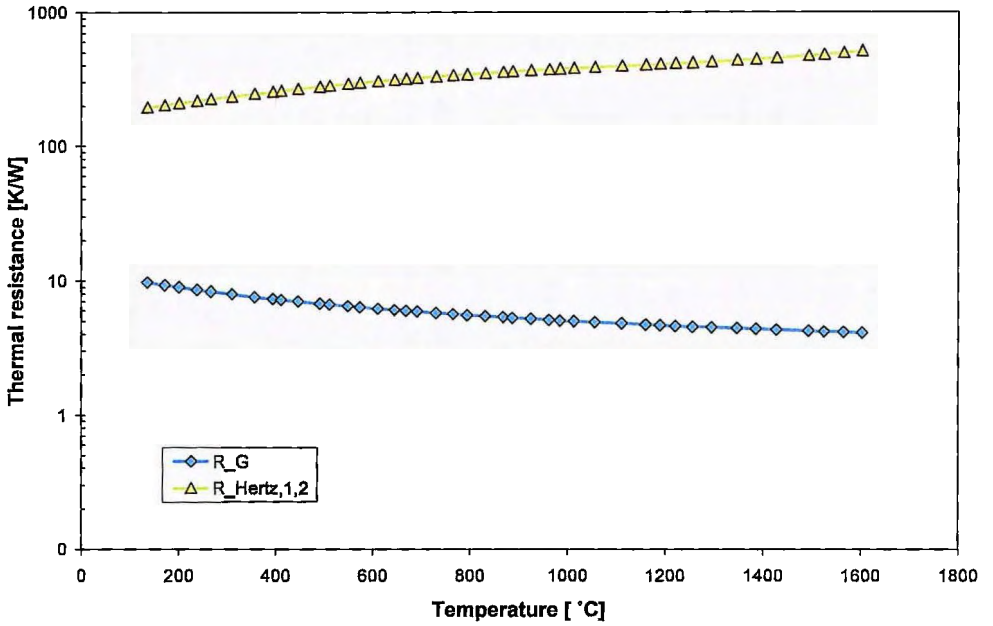

Figure 6.6: Thermal resistance parametrical study in the bulk region

Comparing the radiation component of the Multi-sphere Unit Cell Model, Eq. (5.35), as well as the correlations proposed by Breitbach & Barthels (1980:392), Eq. (3.150), and Robold (1982:156), Eq. (3.165), with experimental data yield the results displayed in Figure 6.7. It should be noted that these aforementioned researchers (Breitbach & Barthels, 1980:392; Robold, 1982:156) also published different sets of experimental data obtained using the same test facility. However, these different experimental data sets deviate at temperatures above 1200°C.

It is evident from Figure 6.7 that Robold (1982:1) fitted his correlation presented in Eq. (3.164) empirically to best represent his data. The correlation proposed by Breitbach & Barthels

(1980:392) is slightly higher than the experimental data at lower temperatures but has a tendency to increase with a lower rate at temperatures above 1400°C.

The Multi-sphere Unit Cell (Radiation component) as shown in Figure 6.7 is calculated by the summation of the short and the long-range radiation components (bottom two lines). It was found that the Multi-sphere Unit Cell Model best represents the experimental data when $3.5 \leq \bar{n}_{long} \leq 4.7$ in Eq. (5.50).

Nonetheless, the Multi-sphere Unit Cell Model demonstrates reasonable accuracy for temperatures below 1200°C but deviates at higher temperatures as shown in Figure 6.7. It is also interesting to note that the long-range radiation component shown in Figure 6.7 is slightly higher in magnitude than the short-range component, and has almost the same gradient (slope). However, this seems to be in contrast to Breitbach & Barthels (1980:392) who stated that in the Zehner & Schlünder (1972:1303) model, the effective thermal conductivity between touching spheres appears to be dominant at higher temperatures, meaning that short-range radiation should be larger at higher temperatures than long-range radiation.

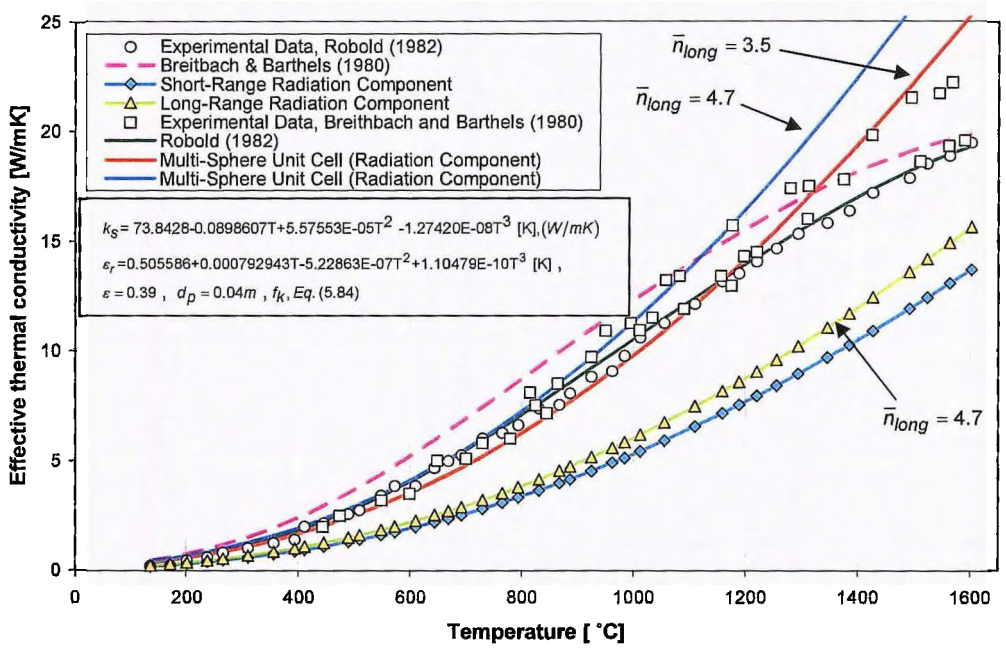

Figure 6.7: Comparison between Multi-sphere Unit Cell Model, Breitbach & Barthels and Robold correlations with experimental data of the High Temperature Oven with graphite spheres at vacuum conditions (Breitbach & Barthels, 1980:395; Robold, 1982:156)

For the Multi-sphere Unit Cell Model, certain assumptions were made that affects long-range radiation; the assumption that the average temperature across the effective long-range pebble $\bar{T}$ is the same as the average temperature over two spheres in contact, and that the non-isothermal correction factor f_k is the same in long-range radiation as for short-range

radiation. In reality is the average temperature $\bar{T}$ going to be higher between the long-range sphere and the sphere under consideration than the assumption previously made, resulting in f_k to decline more sharply at higher temperatures. Improvements can be made to the Multi-sphere Unit Cell Model by deriving a non-isothermal correction factor specifically tailored for long-range radiation using CFD. Therefore, further investigation should be done into long-range radiation to accurately calculate this damping effect at temperatures above 1200°C.

It is also important to note that Figure 5.5 indicated that more spheres contribute to the long-range radiative thermal conductivity than indicated by the coordination flux number $\bar{n}_{long} = 4.7 \approx 5$. However, these low values for $\bar{n}_{long}$ make sense here since the average long-range diffuse view factor $F^{L}_{1-2,avg}$ is actually much higher than it would be for a properly weighted value. Therefore, the long-range coordination flux number $\bar{n}_{long}$ simply compensates for the earlier overestimation.

The second experimental setup of the HTO that is considered is the tests conducted at an elevated pressure $P_g = 70kPa - 85kPa$, using helium as the saturated gas to a temperature of up to 927°C. A curve was fitted through the data by Robold, 1982:160 and extrapolated to higher temperatures, as displayed in Figure 6.8. Again, Robold's (1982:156) model was fitted empirically to best represent his experimental data.

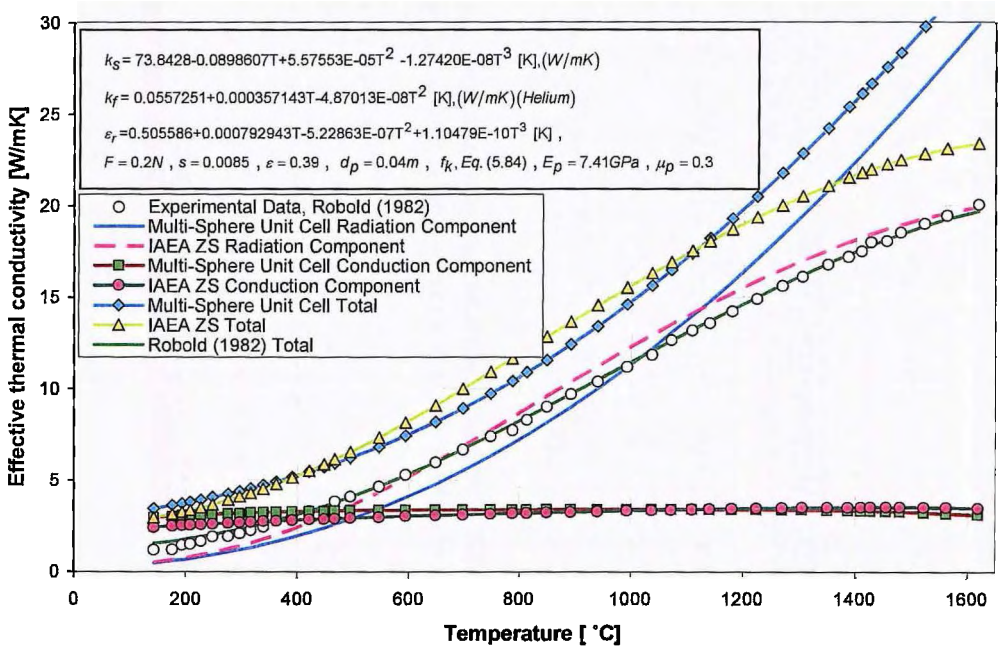

Figure 6.8: Comparison between Multi-sphere Unit Cell Model and the proposed International Atomic Energy Agency correlation with experimental data of the High Temperature Oven, $(\bar{n}_{long} = 4.7)$

The correlation proposed by the Niessen & Ball (2000:301) is also included in Figure 6.8, indicated by IAEA ZS Total representing the summation of Eq. (3.20), Eq. (3.102) and Eq. (3.150), where as the Multi-sphere Unit Cell Total represents the summation of the conduction component Eq. (5.34) and the radiation component Eq. (5.35) using the Hertzian contact network. Robold's results were calculated with Eq. (3.163). Furthermore, a small contact force between the pebbles was assumed due to the packed bed being so small in geometry.

It is interesting to note that both the Multi-sphere Unit Cell Model (Hertzian contact network) and the IAEA ZS Total correlation are higher than the experimental data and intuitively the correlation proposed by Robold (1982:129). One possible reason worth investigating may be the method Robold (1982:129) used to extract the effective thermal conductivity data from experimental results. The Multi-sphere Unit Cell Model and the IAEA ZS Total correlations are in good agreement with each other up to a temperature of 1200°C and thereafter deviate. This can be attributed as previously mentioned to the non-isothermal correction factor for long-range radiation, which is assumed to be the same as for short-range radiation.

6.3 VALIDATION OF MULTI-SPHERE UNIT CELL MODEL IN THE WALL REGION

In this section, the conduction and radiation components of the Multi-sphere Unit Cell Model in the wall region are validated separately and integrally, using data obtained by Kitscha & Yovanovich (1974:93) and Robold (1982:160).

Kitscha & Yovanovich (1974:93) conducted experiments on the overall thermal joint resistances between a steel sphere and a flat surface as presented in Figure C.1. The load was varied to study the effect on overall solid and gas conduction. For each constant load, the gas pressure was also varied from vacuum to atmospheric conditions.

For this study, the experimental test conducted with argon as the interstitial gas was considered. Comparison between experimental results and Eq. (5.68) of the Multi-sphere Unit Cell Model is displayed in Figure 6.9. It should be noted that Kitscha & Yovanovich (1974:93) did not give a root mean square surface slope value, m_{RMS}, so the general correlation of Tanner & Fahoum (1976:299), displayed in Table 3.4, was used to determine m_{RMS} as it gave the best results.

It can be seen that the Multi-sphere Unit Cell Model compares quite well with the experimental results of Kitscha & Yovanovich (1974:93), at higher applied loads. A deviation from the experimental results at an applied load of $F = 16N$ however is observed. This can be attributed to the fact that the correct root mean squared surface slope, m_{RMS}, is not known

as it effect results more at lower applied forces. In addition, it can also be seen that the thermal resistance at $F = 16N$ follows a trend different from its counterparts, at higher applied loads. The highest average percentage difference between the Multi-sphere Unit Cell Model and experimental data, disregarding the $F = 16N$ case, is 9.15%.

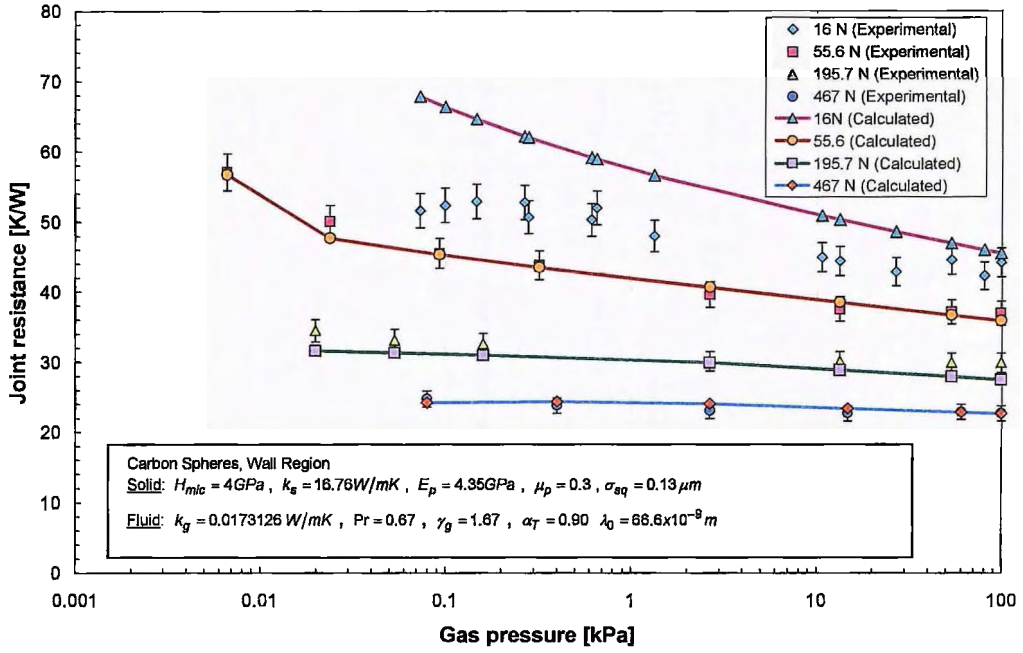

Figure 6.9: Comparison between Multi-sphere Unit Cell Model and Kitscha & Yovanovich experimental data for the wall region (Kitscha & Yovanovich, 1974:93)

The next test that is considered is that conducted by Robold (1982:160) for heat transfer in the wall region at vacuum and elevated pressure (helium) conditions. Comparison of the experimental data with the Multi-sphere Unit Cell Model, Eq. (5.74) and Eq. (5.81), at vacuum conditions leads to Figure 6.10.

Comparison between the experimental data and the Multi-sphere Unit Cell Model in the wall region shows good agreement. It was found that $\bar{n}_{long}^{W} = 1$, with the sphere and wall emissivity assumed to be the same. It is also interesting to note that the long-range radiation in the wall region is much lower than in the bulk region, which is also used for calculations in the near-wall region as previously stated. This confirms that thermal radiation heat transfer in the wall region occurs mainly between the wall and spheres in contact.

Comparison of the experimental data with the Multi-sphere Unit Cell Model, Eq. (5.68), Eq. (5.74) and Eq. (5.81), at elevated pressure conditions (helium) in the wall region led to Figure 6.11. Again, as demonstrated in Figure 6.8, the prediction of the Multi-sphere Unit Cell is higher than the experimental data obtained by Robold (1982:160). As previously mentioned one possible reason worth investigating may be to analyze the method

Robold (1982:129) used to extract the effective thermal conductivity data from experimental results.

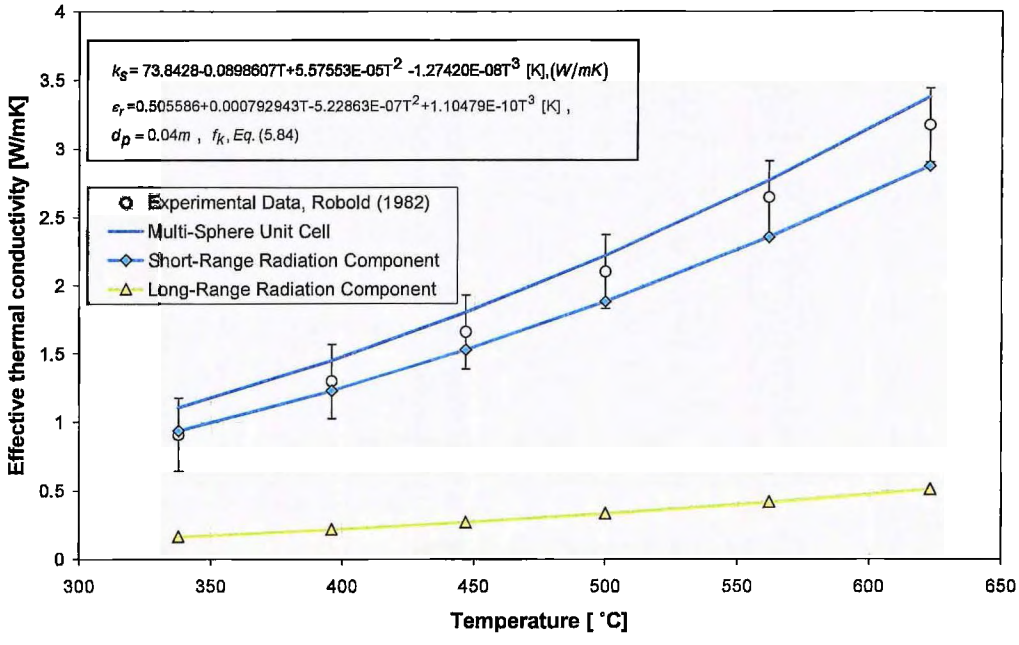

Figure 6.10: Comparison between Multi-sphere Unit Cell Model and experimental data in the wall region at vacuum conditions (Robold, 1982:160)

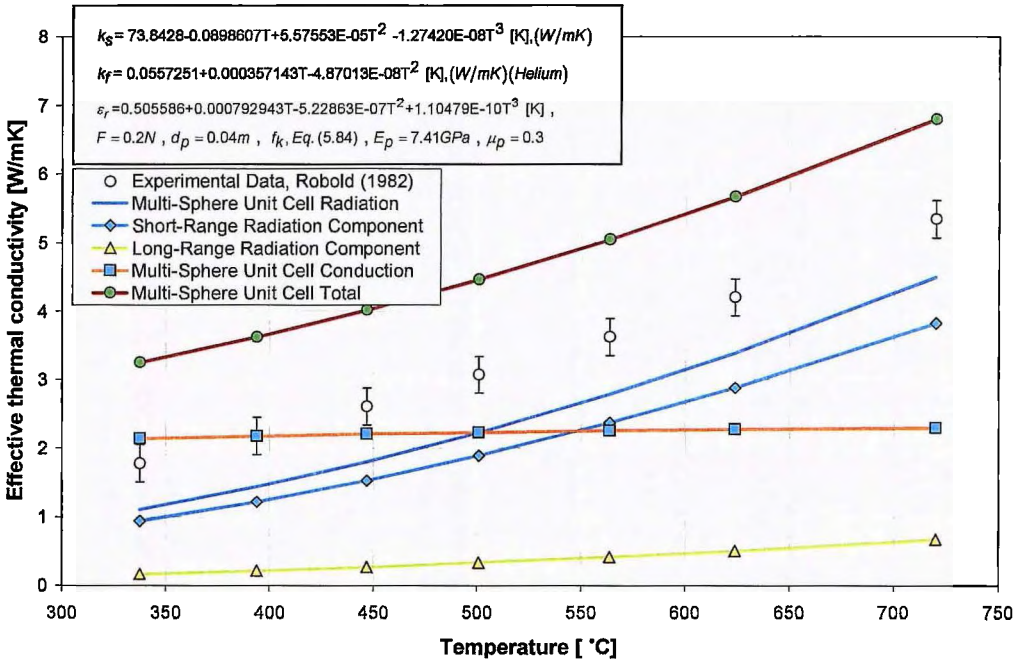

Figure 6.11: Comparison between Multi-sphere Unit Cell Model and experimental data in the wall region at elevated pressure saturated with Helium (Robold, 1982:160)

6.4 VERIFICATION OF THE MULTI-SPHERE UNIT CELL MODEL IN A RANDOMLY PACKED BED

The SANA-I experimental test facility was chosen to compare the experimental effective thermal conductivity results with those predicted by the Multi-sphere Unit Cell Model in a randomly packed bed configuration considering all the integrated effects. The test facility investigated the heat transfer mechanisms inside the core of a pebble bed HTR. A limitation of this experimental data set is that the tests were conducted at a pressure near atmospheric conditions. This results in natural convection flows to occur increasing the effective thermal conductivity, as shown graphically in Appendix C (Figure C.4).

The SANA-I experimental test facility had a central heater element with a diameter of 0.13 m and an outer cylindrical diameter of 1.5 m. Two different sized graphite pebble diameters were used namely $d_p = 60mm$ and $d_p = 30mm$, in a randomly packed arrangement with a bed height of $L_{bed} = 1\,m$. The bed was heated by an electrical resistance graphite heater, as shown in Figure C.4, for which temperature profiles were generated at three different heights.

For this study, the 10 kW and 35 kW long heater element with the pebble diameter of $d_p = 60mm$, saturated with helium is considered. Test results were obtained from Stöcker (1998:34) and are presented in Table C.10 and Table C.11. The isothermal temperature distribution for the 35 kW long heater steady-state is presented in Figure C.5.

The effective thermal conductivity for the SANA-I experimental test facility was previously extracted as a function of temperature only as shown in Niessen & Ball (2000:306). This approach, however, is not suitable to observe any effects that the porous structure may have on the effective thermal conductivity in the radial direction. Therefore, it was decided that the following approach would be used to extract the effective thermal conductivities for the two aforementioned steady-states:

$$k_{eff} = \frac{Q\ln(r_{i+1}/r_i)}{2\pi L_{bed}(T_i - T_{i+1})} \tag{6.7}$$

It should be noted that the more refined approach that was used to extract of the effective thermal conductivity from the HTTU data, Eq. (4.2), could not be applied to the SANA results because there are only eight radial temperature measurements. As Dieck (2007:174) explains, the number of polynomial curve-fit constants must be far less than the number of experimental measurements in any polynomial curve fit and that was not the case for the SANA-I experimental results. Furthermore, it was also decided to extract only the effective thermal conductivity for the temperature profiles measured at heights 0.5 m and 0.91 m. This eliminates any influence the bottom electrode coolers may have on the temperature profiles.

The heat flux $P_{Heating\ Element}$, tabulated in Table C.10 and Table C.12, was used as a constant throughout the packed bed in the radial direction and therefore adiabatic top and bottom boundaries were assumed. This is a valid assumption because Van Antwerpen (2007:121) stated that from sensitivity studies it was found that modelling the top and bottom insulation had a negligible effect on the temperature results. The effective thermal conductivity results are tabulated in Table C.12 and Table C.13 and presented graphically in Figure C.6 and Figure C.7.

Comparison between the Multi-sphere Unit Cell Model and other correlations are compared with the SANA-I experimental results obtained from Niessen & Ball (2000:306) as a function of temperature, is shown in Figure 6.12. The coordination flux number for the long-range radiation was taken as $\bar{n}_{long} = 4.7$. This is also done for all the analyses presented in the remainder of this chapter. The contact force distribution was taken to be the same as that of the HTTU (Eq. D.49) due to the close geometrical proximity of the pebbles and packed bed.

When comparing the effective thermal conductivity simulation results with the experimental data given in Figure 6.12, it must be remembered that heat is transported not only by thermal conduction and radiation, but also by natural convection in the pebble bed. Natural convection in the SANA-I experimental test facility was not suppressed as the developers of the test facility wanted to measure how natural convection assists in the decay heat removal process. This explains why the majority of the correlations presented in Figure 6.12 are somewhat lower than the measured values (Niessen & Ball, 2000:302).

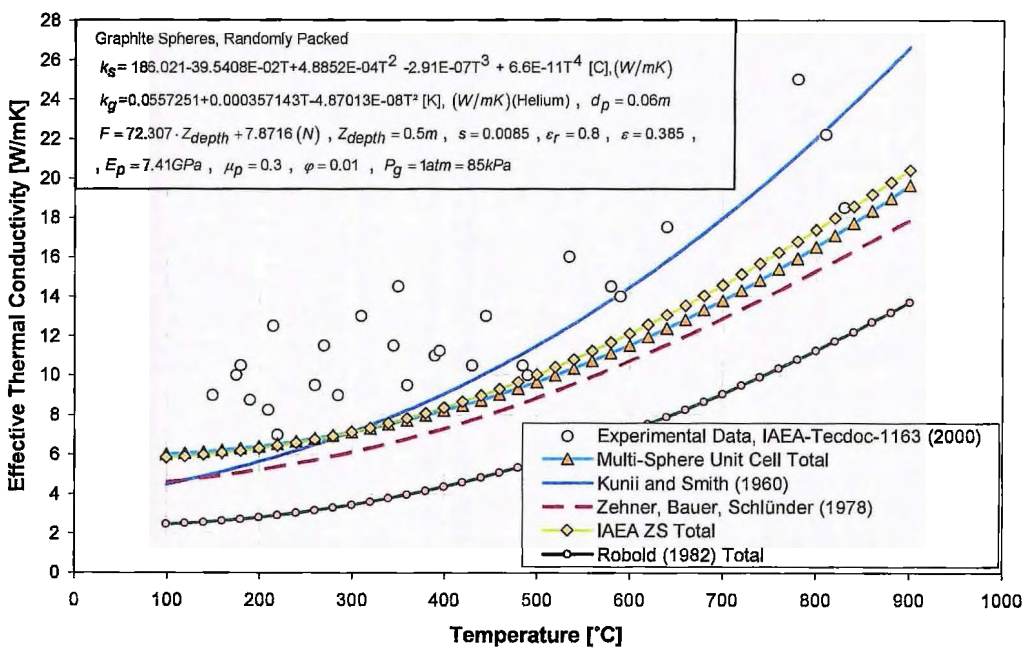

Figure 6.12: Comparison between various correlations and SANA-I experimental data versus temperature saturated with helium. (Niessen & Ball, 2000:306)

Figure 6.12 demonstrates that the IAEA ZS Total, the ZBS presented in Eq. (3.89), and the Multi-sphere Unit Cell Model are in close agreement with each other. The ZBS correlation deviates slightly due to the contact area fraction parameter φ being unknown for the packing. However, the model proposed by Kunii & Smith (1960:71), Eq. (3.130), somewhat over-predicts the effective thermal conductivity, while the correlation proposed by Robold (1982:156) under-predicts the values.

In Figure 6.13, the two different components of the Multi-sphere Unit Cell Model are demonstrated. It should be noted that the contribution of thermal radiation is only the dominant factor at temperatures above 500°C for a packed bed saturated with helium gas. This emphasises that the effective thermal conductivity due to conduction $k_e^{g,c}$ should not be discarded in any effective thermal conductivity analysis and that the accurate simulation thereof is important, especially at lower temperature.

It is evident from Figure 6.13 that the effect the near-wall and wall regions have on the effective thermal conductivity measurements can not be clearly distinguished. Therefore, the effective thermal conductivity measurements were extracted in the radial direction as previously mentioned and the comparative results for the 10 kW steady-state are displayed in Figure 6.14.

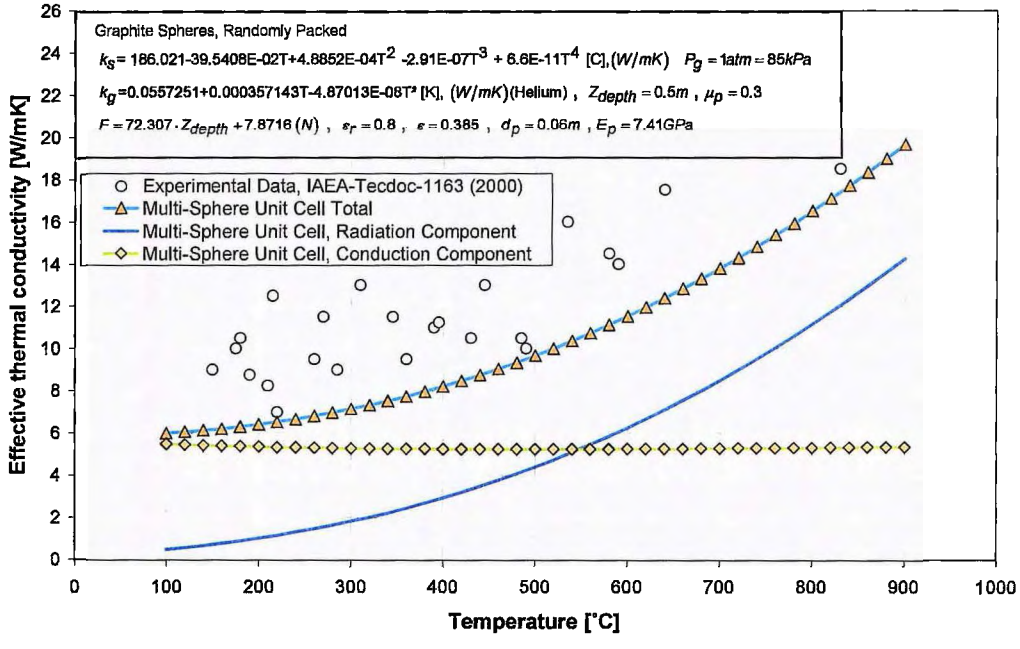

Figure 6.13: Comparison between the Multi-sphere Unit Cell Model components and SANA-I effective thermal conductivity experiment, experimental results (Niessen & Ball, 2000:306)

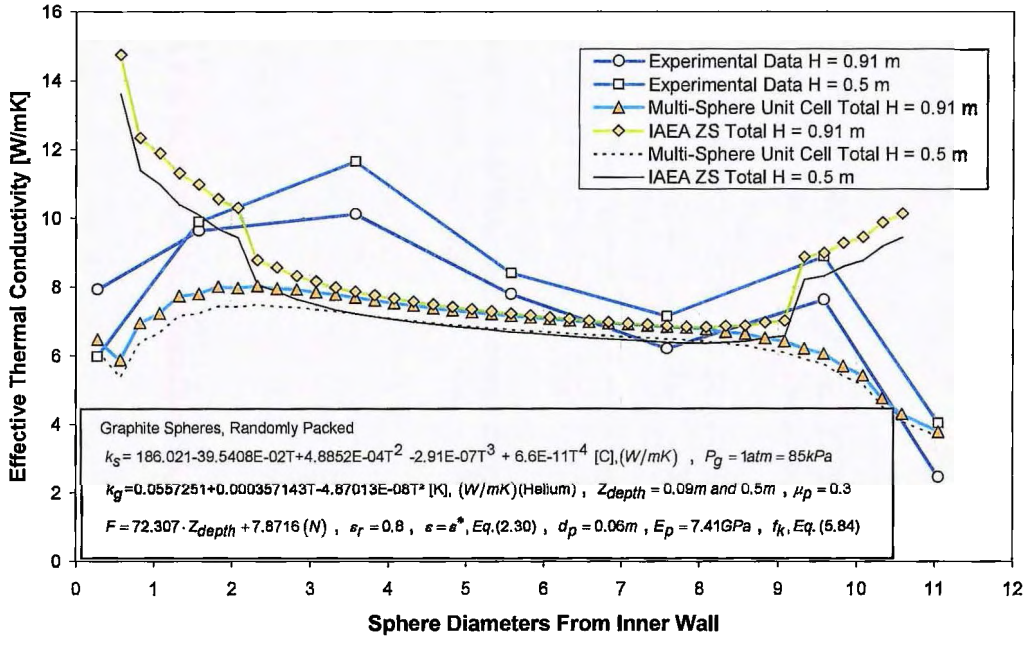

Figure 6.14: Comparison between effective thermal conductivity correlations and experimental results of the SANA-I experimental test facility for the 10 kW steady-state

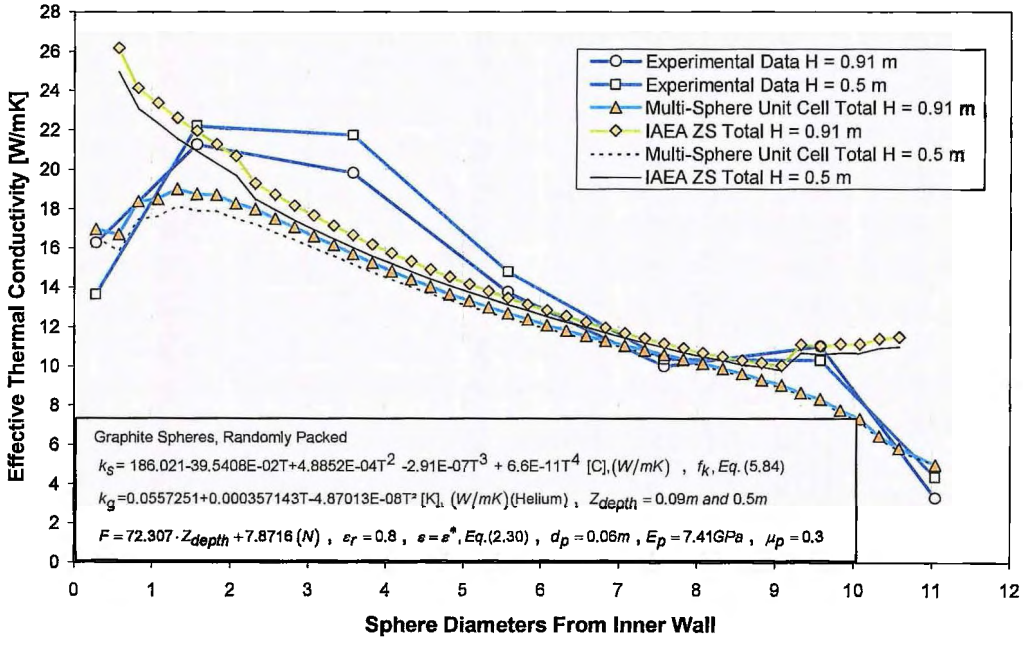

Figure 6.15: Comparison between effective thermal conductivity correlations and experimental results of the SANA-I experimental test facility for the 35 kW steady-state

In Figure 6.14, the effect of natural convection can be seen more profoundly with the effective thermal conductivity peaks at $3.5d_p$ and $9.5d_p$ sphere diameters from the inner wall. It is also demonstrated that the IAEA ZS Total correlation fails in the near-wall region where the Multi-sphere Unit Cell Model captures the expected decrease in effective thermal conductivity in the near-wall region. However, the effective thermal conductivity right next to the inner wall shows a slight increase from that slightly away from the wall. The comparative results for the 35 kW steady-state test can be seen in Figure 6.15.

It can be seen in Figure 6.15 that the IAEA ZS Total correlation again breaks down in the wall region. It is interesting to note that from the study in Figure 6.16 a slight increase in effective thermal conductivity (conduction) of the Multi-sphere Unit Cell Model at the inner wall is evident, where thermal radiation decreases. This phenomenon is also evident in the conduction component of the Multi-sphere Unit Cell Model in the 10 kW steady-state case (not shown).

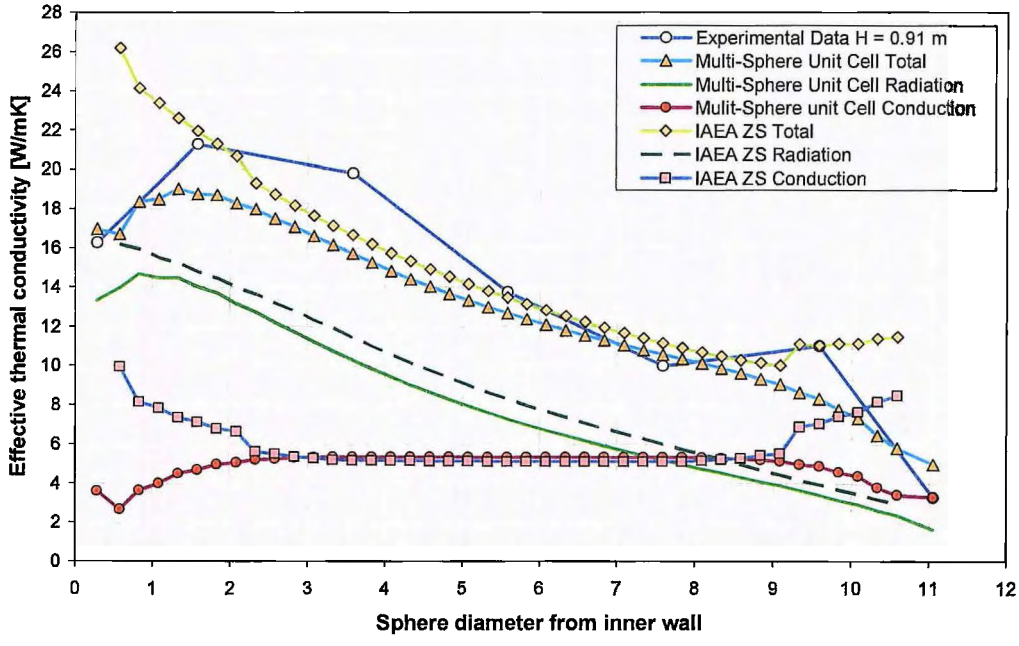

Figure 6.16: Comparison between effective thermal conductivity correlations (components) and experimental results of the SANA-I experimental test facility for the 35 kW steady-state

There are two important issues that must be raised for the simulation of the effective thermal conductivity at the "inner reflector" of the SANA-I experimental test facility.

Firstly, it must be mentioned that thermal radiation was found from analysis to be the dominant heat transfer mechanism in both of the aforementioned cases at the "inner reflector". The Multi-sphere Unit Cell Model (radiation component) for the wall region, Eq. (5.81), was developed based on an almost flat wall surface. In general, the packing in the

inner wall region for the SANA-I experimental facility is different from that of a flat surface since the "inner reflector" actually consisted of a single heater electrode with a severe curvature, as illustrated in the exact scaled representation in Figure 6.17. This would entail a much lower diffuse view factor between the "inner reflector" and the sphere in contact, resulting in a much lower contribution to the effective thermal conductivity by thermal radiation. This phenomenon will result in the summation of the radiation and conduction component to be much lower.

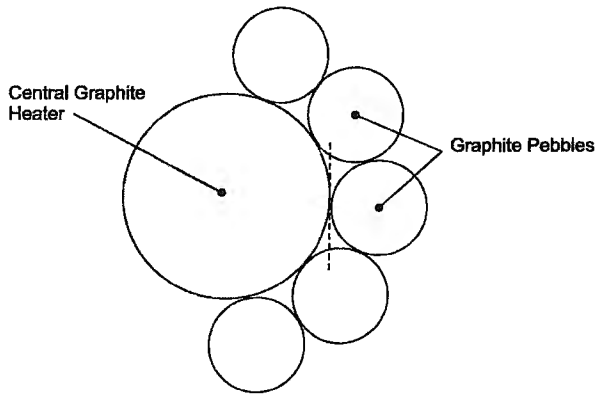

Figure 6.17: Packing structure in the inner region of the SANA-I experimental test facility

Secondly, it is noted that an increase in the conduction component of the Multi-sphere Unit Cell Model exist at the "inner reflector". This make sense due to the fact that conduction mostly occurs through the bulk gaseous region as displayed in Figure 6.6 with the low R_G thermal resistance. The increase in the conduction effective thermal conductivity occurs due to the porosity increasing to one, which intuitively means more gas to conduct through. This increase will not be as profound if nitrogen was used as the gas medium due to a much lower gas thermal conductivity. That said, the effective thermal conductivity prediction in the outer wall region compares better with the measurements of Figure 6.14 and Figure 6.15.

The last comparison between the effective thermal conductivity correlations and experimental results is done by considering the HTTU. Comparative results for Tests 1 and 2 for the 20 kW steady-state are displayed in Figure 6.18 and Figure 6.19, and results for the 82.7 kW steady-state are displayed in Figure 6.20 and Figure 6.21.

It should be noted that no decrease of effective thermal conductivity in the near-wall region is visible in the experimental results for the extraction of the effective thermal conductivity measurements in level C (Figure 6.18, Figure 6.19). Therefore, the effective thermal conductivity was also extracted for thermocouples on level D for the first test done at the 20 kW steady-state as shown in Figure 6.18. This however can only be done for the first 20 kW steady-state test, due to the thermocouples being out of order thereafter. Nonetheless, the effective thermal conductivity values on level D show that there is a declination in effective thermal conductivity on the 20 kW steady-state as well.

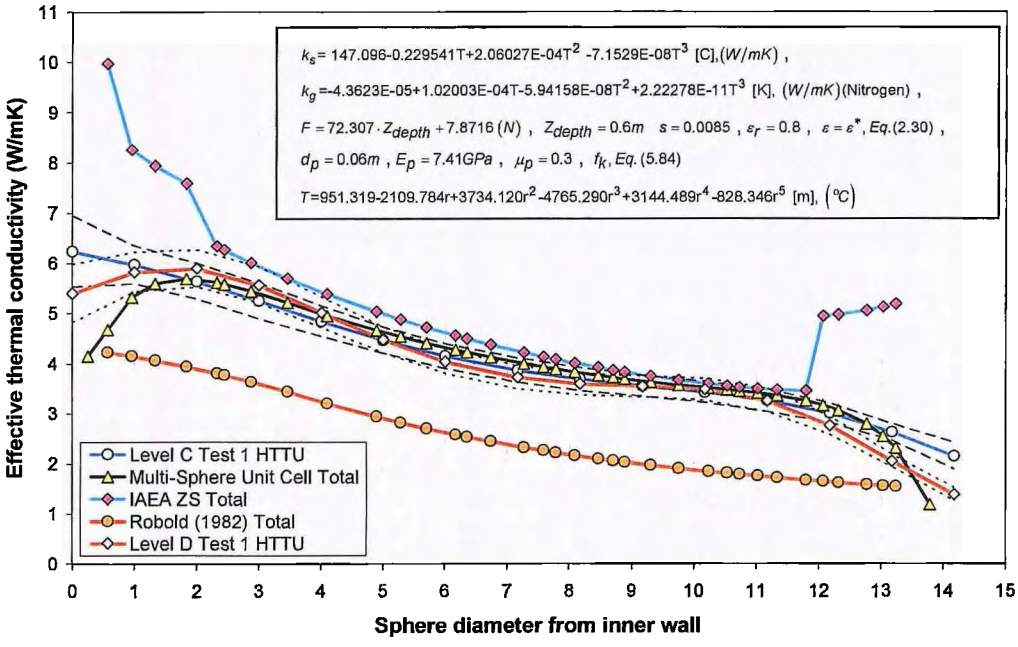

Figure 6.18: Comparison between effective thermal conductivity correlations and experimental results of the High Temperature Test Unit experimental test facility for the 20 kW steady-state, Test 1

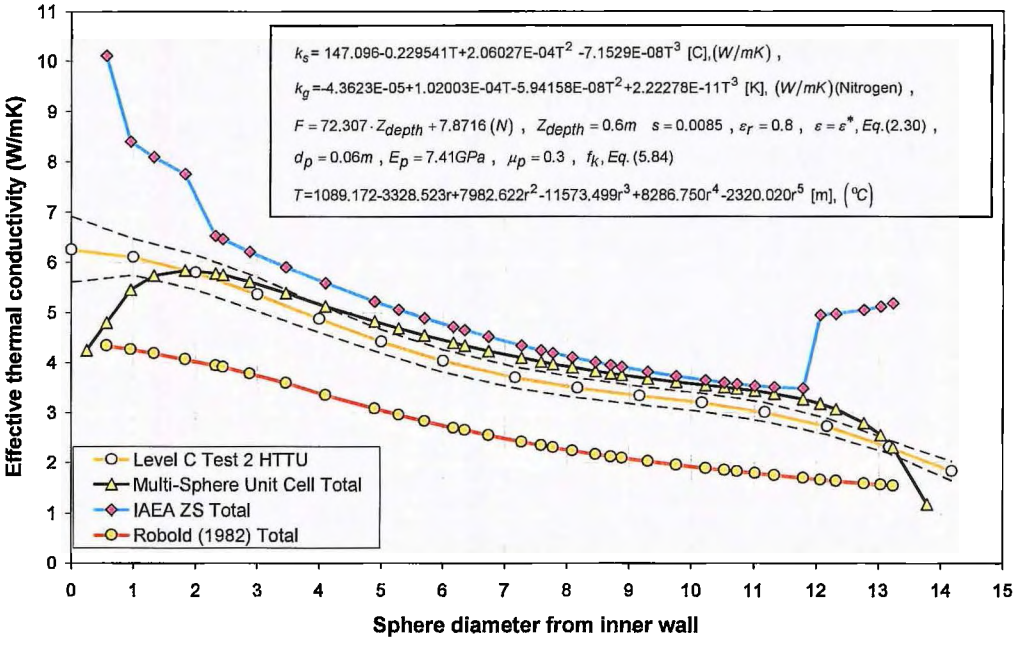

Figure 6.19: Comparison between effective thermal conductivity correlations and experimental results of the High Temperature Test Unit experimental test facility for the 20 kW steady-state, Test 2

From Figure 6.18 and Figure 6.19 it can be seen as in the case for the SANA-I experimental test facility, that the IAEA ZS Total correlation breaks down when entering the near-wall region. It is interesting to note that in the region of $2d_p$ and $11.8d_p$ the effective thermal conductivity of the IAEA ZS Total correlation changes rapidly (also seen in Figure 6.14 and Figure 6.15). This is due to the contact area conduction parameter k_e^c, Eq. (3.102), not being a continuous function with varying porosity that lead to a rapid increase when porosity fell into FCC range changing the parameters displayed in Table 3.2 and Table 3.3.

In contrast, the Multi-sphere Unit Cell Model demonstrates a decrease in effective thermal conductivity when entering the near-wall region. It is unclear why the Multi-sphere Unit Cell Model under-predicts the experimental effective thermal conductivity in the near-wall and wall regions. However, one possible cause, worth investigating, is that the test was conducted at 10 kPa and not total vacuum. Although the system pressure is very low, natural convection cannot be disregarded entirely. Therefore, a further investigation should be done to analyzing the effect of natural convection in the HTTU. Another cause worth investigating is the impact $k_{f,eff}$ has on the experimental effective thermal conductivity. The correlation proposed by Robold (1982:156) again under-predicts the effective thermal conductivity results.

Comparison between the Multi-sphere Unit Cell Model and the IAEA ZS Total correlation with the 82.7 kW steady-state test cases shows good comparison with the experimental data, displayed in Figure 6.20 and Figure 6.21. Again, it can be seen that for both test cases the simulated effective thermal conductivity results in the near-wall and wall regions obtained with the Multi-sphere Unit Cell Model is slightly lower than that determined experimentally and that the correlation proposed by Robold (1982:156) under-predicts the effective thermal conductivity. A breakdown of the different components for the Multi-sphere Unit Cell Model and the IAEA ZS Total correlations is shown in Figure 6.22.

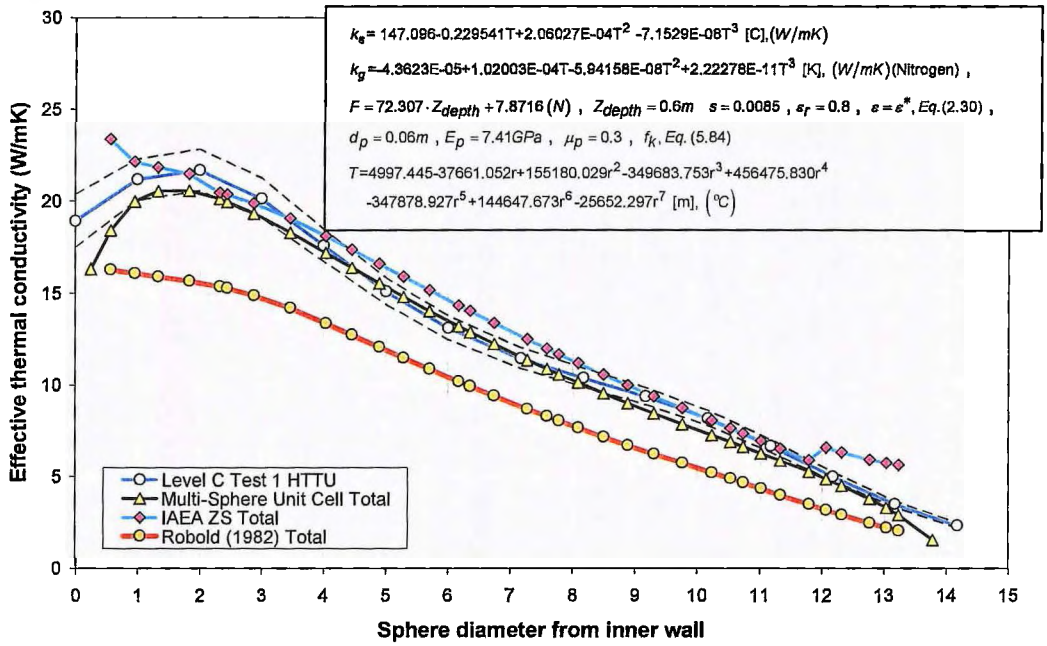

Figure 6.20: Comparison between effective thermal conductivity correlations and experimental results of the High Temperature Test Unit experimental test facility for the 82.7 kW steady-state, Test 1

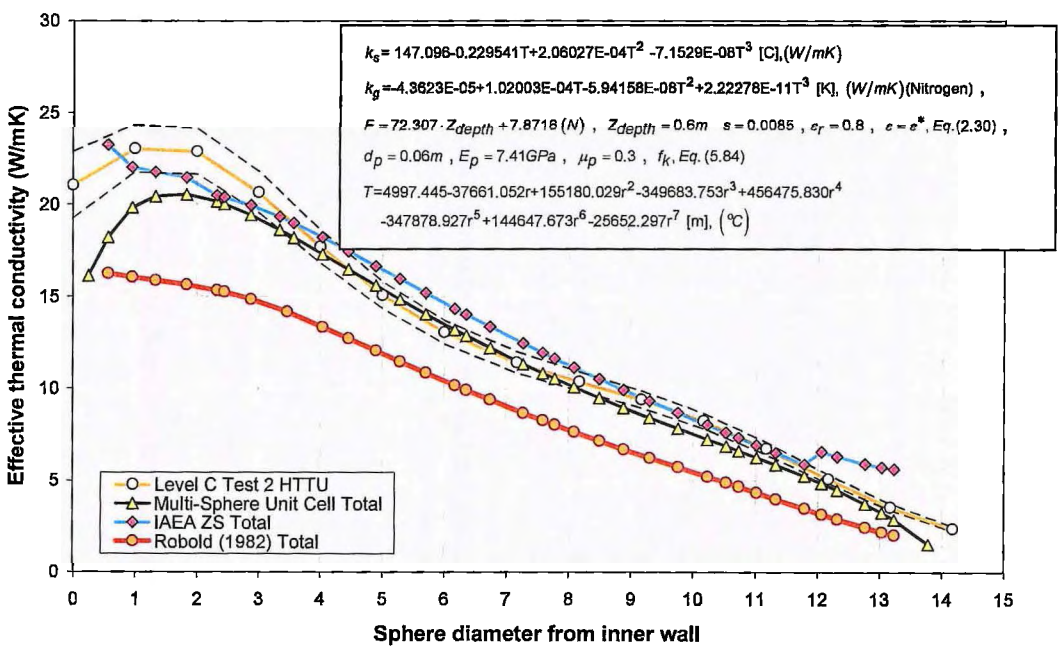

Figure 6.21: Comparison between effective thermal conductivity correlations and experimental results of the High Temperature Test Unit experimental test facility for the 82.7 kW steady-state, Test 2

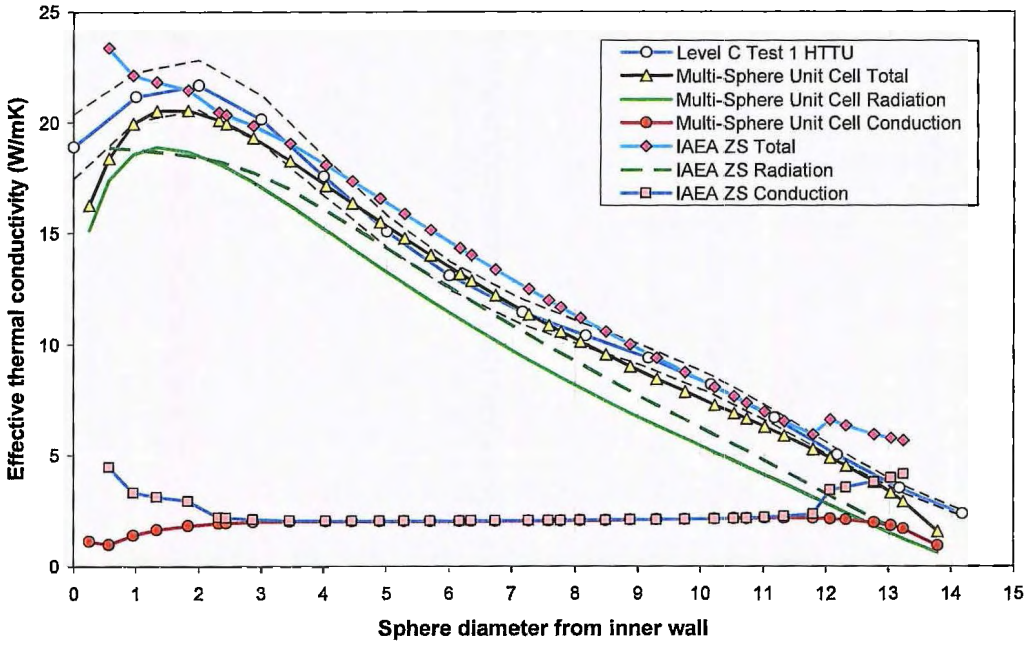

Figure 6.22: Comparison between effective thermal conductivity correlations (components) and experimental results of the High Temperature Test Unit experimental test facility for the 82.7 kW steady-state, Test 1

6.5 CONCLUSION

This chapter presented the verification and validation of the separate components of the Multi-sphere Unit Cell Model as well as the integrated model by comparing predicted results with that of various experiments. Good comparison between experimental data and the conduction component of the Multi-sphere Unit Cell Model was achieved. In addition, the radiation component of the Multi-sphere Unit Cell Model for temperatures below 1200°C appears to be promising. However, some uncertainty still arises for temperatures above 1200°C. This uncertainty can be attributed to several assumptions that were made: the non-isothermal correction factor is assumed to be the same as that of short-range radiation, the average temperature between the long-range pebble and the pebble under consideration is assumed to be the same as that of two adjacent spheres and the long-range diffuse radiation view factor used is only an average, unweighted view factor. Also caution should be taken when simulating effective thermal conductivity for lower solid material thermal conductivity values. This is because the non-isothermal correction factor is only valid for a specific range of $1/\Lambda_s$. Improvements were proposed to the Multi-sphere Unit Cell Model to increase the applicability above 1200°C and for lower solid conductivity materials; deriving a non-isothermal correction factor specifically tailored for long-range radiation and extending the range of $1/\Lambda_s$. Both can be done with CFD.